In-plane resistivity and an explanation for the characteristic T^* in high-T_c cuprates

George A. Levin and Khandker F. Quader
Department of Physics, Kent State University, Kent, Ohio 44242
(Received 9 August 2000)

We offer an explanation for the observed crossover temperature T^* in in-plane resistivity ρ_{ab} of biplanar high-T_c cuprates. The key to our picture is the existence of nondegenerate and degenerate carriers possessing different quasiparticle relaxation rates. In the underdoped regime the change of slope $d\rho_{ab}/dT$ at T^* results from the thermal activation of nondegenerate carriers. In the overdoped regime, the nondegenerate carriers tend to become degenerate and a second small Fermi energy emerges, resulting in a change to T^2 behavior in ρ_{ab} at low T. We compare our results with data on several compounds. We also find an approximate scaling in conductivity.

I. INTRODUCTION

The unusual normal-state properties of the high-T_c cuprate superconductors are yet to be well understood. The evolution of the normal state with doping is marked by some extraordinary universal features. It is recognized that an understanding of these unusual features is important to the understanding of superconductivity at high temperatures. The temperature (T) dependence of properties, such as in-plane resistivity $\rho_{ab}(T)$, Hall coefficient $R_H(T)$, electronic spin susceptibility $\chi_s(T)$, entropy $S(T,x)$, optical conductivity, etc. in the *underdoped* cuprates reveal a *characteristic* temperature T^*, that demarcates high-T and low-T behavior. In this region, T^* decreases with increased doping (in anticorrelation with the critical temperature T_c), and almost vanishes at or near optimal doping defined by maximum of T_c. In the *overdoped* region, the T dependence of ρ_{ab} approaches the usual Fermi-liquid (FL) behavior with some subtle differences. Examples of materials which show these types of behavior are $Bi_2Sr_2CaCu_2O_{8+\delta}$,[1] $Bi_2Sr_2Ca_{1-x}Y_xCu_2O_2$,[2] $Y_{1-x}Pr_xBa_2Cu_3O_{7-\delta}$,[3] $Tl_2Ba_2CuO_{6+\delta}$,[4] etc.

Here we focus on the temperature and doping dependences of in-plane resistivity $\rho_{ab}(T,x)$. At a given temperature, ρ_{ab} decreases monotonically with an increasing number of holes. In the *underdoped* cuprates,[1–3,5] the slope $d\rho_{ab}/dT$ changes appreciably within a narrow range of temperature around $T^*(x)$. At $T>T^*$, ρ_{ab} changes approximately linearly with temperature, but not as rapidly as it does for $T<T^*$. The crossover temperature $T^*(x)$ decreases with increasing number of holes, and at *optimal* doping ρ_{ab} exhibits a linear-T behavior down to T_c, with no apparent change of slope ($d\rho_{ab}/dT=\text{const}$). In *overdoped* samples, ρ_{ab} exhibits[4,6] a T^2 behavior at low temperatures, and possibly some power higher than linear T at higher temperatures.

The evolution of $\rho_{ab}(T,x)$ correlates with that of $\chi_s(T,x)$ and the electronic entropy $S(T,x)$.[7,8] With decreasing temperature $\chi_s(T,x)$ decreases in the underdoped and increases in the overdoped samples. The crossover temperature marking the transition between high and low-T behavior exhibits the same anticorrelation with T_c as it does in resistivity. A detailed discussion of experimental results on susceptibility and electronic entropy within the context of the same model that is presented here is given in Ref. 9.

Over the past years, several theoretical approaches have been taken to address these issues and the nature of the crossover of the physical properties of the cuprates at T^*. In attempts to explain transport properties, and in particular, the linear-T in-plane resistivity (at optimal doping), theories based on extensions of Fermi-liquid theory (FLT),[10,11] as well as, on non-FL concepts[12] have been proposed. The concepts of ''spin gap''[13] or ''pseudogap''[14] have been proposed to explain observed features in $\rho_{ab}(T,x)$ and $\chi_s(T,x)$ in the underdoped regime. A central aspect of many of the more FL-like theories is the existence of anomalous electron relaxation rates in the cuprates. Some of these theories have at their core the concepts of ''hot spot''[11,15] or ''cold spots''.[16] While these theories have had varying degrees of success, it has proved to be difficult to explain the evolution of the properties across the full range of doping (underdoped to optimal to overdoped).

In this paper, we present an alternate, and rather different approach to understanding the origin of the crossover temperature T^* in the cuprates. We argue that calculations based upon the basic features of our model proposed earlier,[17] support the point of view that the crossover temperature T^* is a signature of an underlying *small* energy scale in the underdoped regime. This decreases with increased carrier density. Beyond optimal doping, our model, in a natural fashion, suggests that the system evolves into a Fermi liquid. The small energy scale in the underdoped regime goes over to one that is then related to the small Fermi energy of the second, emerging Fermi surface in the overdoped regime. Here we concentrate on in-plane resistivity, and compare our results with data on a number of materials in the underdoped, optimal, and overdoped regimes.

The key aspects of our model are (a) the presence of nondegenerate (and hence really non-FL like), as well as degenerate (FL like) carriers (denoted as η and ξ components, respectively); (b) the nondegenerate and degenerate carriers possess different relaxation rates; viz. $\tau_\eta^{-1}\propto T^2$, and $\tau_\xi^{-1}\propto T$.[17] Thus the model is quite different from the models based on two degenerate bands,[18] which we believe cannot reproduce the properties of cuprates being considered here. The idea that two relaxation rates affect transport properties of the cuprates was proposed earlier on by Anderson.[19] A

point to note in our model is that the quasiparticles with the longer lifetime $\tau_\eta \propto T^{-2}$ are substantially less numerous than those with the shorter lifetime $\tau_\xi \propto T^{-1}$. Then at optimal doping, the density of carriers $n_\eta \propto T$, while $n_\xi = \text{const} \gg n_\eta$. As a result, the contributions of both components to in-plane conductivity is of the same order of magnitude and have similar T dependence: $\sigma_{xx} \propto n_\xi \tau_\xi + n_\eta \tau_\eta \propto 1/T$. However, the off-diagonal component of the conductivity, is dominated by the component with higher mobility: $\sigma_{xy} \propto n_\eta \tau_\eta^2 \propto 1/T^3$, and this leads to the T-dependent Hall coefficient $R_H \sim \sigma_{xy}/\sigma_{xx}^2 \propto 1/T$ and $\cot \theta_H = \sigma_{xx}/\sigma_{xy} \propto T^2$.[17]

At this time we do not have a microscopic calculation which would explicitly give rise to degenerate and nondegenerate carriers. There are, however, several justifications: Experiments do not rule out more than one type of carriers that are characterized by different relaxation rates. Some of the other theories[11,15,16] have in a way more than one ''entity'' in that they possess different relaxation rates, and hence contribute in a different manner to transport. In the more recently proposed ''cold spots'' model,[16] a small number of carriers have a substantially longer lifetime than the majority of quasiparticles. The main difference between this work and ours is the placement of the high mobility component. We attribute the minority component to a band almost completely submerged below the Fermi level, so that these quasiparticles are nondegenerate and, correspondingly, their number density is small and T dependent, $n_\eta \propto T$. In Ref. 16, the longer lived carriers are assumed to exist on narrow segments of the Fermi surface with the same result that their number density is small and $\propto T$. However, we believe that our model, schematic as it is in nature, contains or mimics the essential features requisite for successfully accounting for the variation of the transport properties across the whole range of doping levels, and providing an explanation for the characteristic underlying energy scale, manifested as the characteristic temperature T^*, in the biplanar cuprates. We are also motivated by our previous results based on this model on the evolution of $\chi(T,x)$, entropy $S(T,x)$, and Hall coefficient $R_H(T,x)$.[9,20]

The paper is organized as follows: In Sec. II we present the basic features of our model proposed sometime back. In Sec. III we outline our calculation of in-plane resistivity for the degenerate and nondegenerate carriers, and show how the quintessential energy scale $W(x)$ emerges within the model. In Sec. IV we discuss our results for under-, optimally, and over-doped regimes. A detailed comparison with data on several cuprates is presented in Sec. V. Also in this section, we show that the data support an approximate scaling in conductivity predicted by theory. We end with concluding remarks in Sec. VI.

II. MODEL

The main idea behind our approach is that the transport properties of the cuprates may be described in terms of *nondegenerate* and *degenerate* carriers, that also possess different relaxation rates. Then in the range of superconducting stoichiometry the anomalies of the normal state result from the presence of a nondegenerate component of charge carriers.[9,17,20] This appears when the chemical potential μ is tuned by doping in the vicinity of the top of the lower quasi-

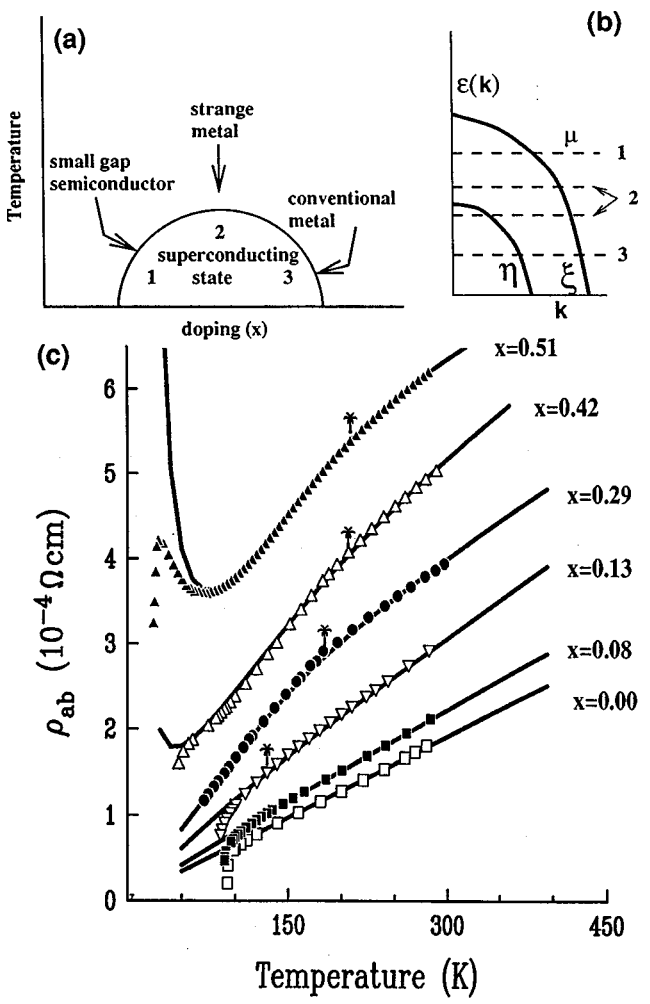

FIG. 1. (a) Schematic temperature-doping phase diagram showing underdoped (1), optimally doped (2), and overdoped (3) regimes. (b) The degenerate ξ and the nondegenerate η bands; (1,2, 3) indicate the locations of the chemical potential μ that correspond to the three regimes in (a). (c) The resistivity of $Y_{1-x}Pr_xBa_2Cu_3O_{7-\delta}$ single crystals. The palm signs indicate the change of slope at $T = T^*(x)$. The solid lines are calculated on the basis of Eq. (13) with $W(x)$ shown in Fig. 3(a).

two-dimensional (2D) band $\epsilon_\eta(0)$; Fig. 1(b). The energy spectrum $\eta_{\mathbf{k}} = |\epsilon_\eta(\mathbf{k}) - \mu|$ of these carriers varies strongly with doping x and temperature T as μ moves relative to $\epsilon_\eta(0)$. The upper band with a large Fermi surface gives rise to a degenerate component (ξ) with a regular Fermi-liquid-type spectrum $\xi_k \approx v_F|k - k_F|$. According to Fig. 1(b), the underdoped regime corresponds to $\mu > \epsilon_\eta(0)$, so that excitation of holes in the η band requires a finite activation energy $\sim \mu - \epsilon_\eta(0)$; this acts like a ''gap.'' As a result, this component freezes out at $T \ll \mu - \epsilon_\eta(0)$. The strongly overdoped regime corresponds to μ going well below $\epsilon_\eta(0)$ due to the increasing number of holes on the CuO_2 planes. At sufficiently low temperatures, $T \ll \epsilon_\eta(0) - \mu$, the nondegenerate component tends to become degenerate, and there emerges a second small Fermi surface with Fermi energy $\sim \epsilon_\eta(0) - \mu$. Thus, in this scenario there is a relatively small, *positive* or *negative*, doping-dependent energy parameter $W(x) \sim \mu - \epsilon_\eta(0)$ that governs the temperature dependences of the properties. We try to show that the experimentally observed

curvatures of $\rho_{ab}(T)$ in underdoped and overdoped regimes are governed by the difference $W(x)$ between the chemical potential and the top of the lower band.

Regarding the relaxation rates of the carriers, it is known that experiments point to the existence of two different relaxation rates in the cuprates. The difference in the temperature dependence of resistivity $\rho_{ab}\sim T$ and the Hall angle[21] $\cot\theta_H\sim T^2$ has been interpreted in terms of normal ($\tau_{\rm tr}\sim T$) and parallel to the Fermi surface ($\tau_H\sim T^2$) relaxation rates.[19] However, the second relaxation rate appears not only in magnetotransport, but also in transient thermoelectric effect.[22] Elsewhere we have presented arguments for attributing different rates to our degenerate (ξ) and nondegenerate (η) components, and showed[17,20] how they explain the coexistence of linear resistivity and the T^2-Hall angle. Based on these considerations, we take

$$\hbar\tau_\xi^{-1}\sim k_BT;\quad \hbar\tau_\eta^{-1}\sim (k_BT)^2/\tilde{E}, \tag{1}$$

where $\tilde{E}$ is a characteristic energy $\sim$0.1 eV.

III. CALCULATION OF IN-PLANE RESISTIVITY

We obtain the normal-state conductivity of both components from the Boltzmann equation in the relaxation time approximation:

$$\sigma_{xx}^i=-\frac{2e^2}{\hbar^2}\sum_{\mathbf{k}}\ \tau_i v_{x,i}^2(\mathbf{k})\frac{\partial f}{\partial\epsilon_{\mathbf{k}}^i}, \tag{2}$$

where $i=\xi,\eta,\tau_i^{-1}$ are the corresponding transport relaxation rates, $v_{x,i}(\mathbf{k})=\partial\epsilon_{\mathbf{k}}^i/\partial k_x$, and $f_i(\epsilon)=[e^{\beta(\epsilon_i-\mu)}+1]^{-1}$ is the Fermi distribution ($\beta=1/k_BT$).

First, we consider the contribution of the nondegenerate (η) component. Since μ is close to $\epsilon_\eta(0)$, we may approximate $\epsilon_\eta(\mathbf{k})$ by a parabolic dependence, which leads to Drude-type conductivity. The number of holes in the η band[9]

$$n_\eta=2\nu_\eta k_BT\ln(1+Z), \tag{3}$$

where $Z=\exp(-\beta\mu)$ is the fugacity, and $\nu_\eta=$const is the two-dimensional (2D) density of states (DOS) in the η band. Hereafter, energy and μ are measured relative to $\epsilon_\eta(0)$. Then, using Eq. (1) we obtain

$$\sigma_{xx}^\eta=\frac{e^2n_\eta\tau_\eta}{m}=\frac{2e^2\nu_\eta\hbar\tilde{E}}{mk_B}\frac{1}{T}\ln(1+Z). \tag{4}$$

The temperature dependence of the fugacity is determined by the mechanism of doping. In our view (Ref. 9), the least ambiguous class of bilayer cuprates are the ones in which the number of holes is controlled by heterovalent substitutions inside the bilayer, such as $Bi_2Sr_2(Ca_{1-x}Y_x)Cu_2O_{8+\delta}$, $TlSr_2(Lu_xCa_{1-x})Cu_2O_y$, etc.

Thus we consider that in these cuprates the total number of holes per bilayer $n_h=n_\xi+n_\eta$ is temperature independent and decreases with x at a constant rate $dn_h/dx=-\kappa N_s$, where κ is the difference between the valences of Y-Ca, Lu-Ca, etc. and N_s is the areal density of these sites (n_ξ and n_η are the number of holes in the respective bands). Then, we obtain for the fugacity:[9]

$$Z(1+Z)^\lambda=e^{-W(x)/T}, \tag{5}$$

where $\lambda\equiv\nu_\eta/\nu_\xi$ is the ratio of the DOS for the two subbands, and

$$W(x)=\Gamma(x-x_0);\ \ \Gamma=\kappa N_s/2\nu_\xi. \tag{6}$$

$W(x)$ is the energy scale that determines the temperature and doping dependence of the chemical potential $\mu(T,x)$ and other properties. Its linear dependence on x follows from that of the total number of holes n_h. The parameter x_0 is the doping level at which the chemical potential is close enough to the top of the submerged band and changes with temperature such that the fugacity is T independent [Eq. (5)].

In the underdoped regime, which corresponds to $W(x)>0$, and at sufficiently low temperature such that $Z\ll1$, the chemical potential becomes T independent, $\mu(x)=W(x)>0$. Thus, the positive $W(x)$ for $T\ll W$ equals the activation energy or the ''energy gap'' for the holes in the nondegenerate η band. The overdoped regime ($x<x_0$) is defined as the doping level at which $W(x)<0$. Correspondingly, at sufficiently low temperature $Z\gg1$ and $\mu(x)=W(x)/(1+\lambda)<0$. The negative $W(x)$ for $T\ll|W|$ determines the second small Fermi energy $\approx|W|/(1+\lambda)$ for the emerging second Fermi surface.

It should be noted that in literature the underdoped and overdoped regimes are usually defined with respect to the values of the critical temperature. Our definition of these regimes is based on the normal-state properties. These two definitions are closely correlated, as discussed below, but not necessarily identical. In other words, the doping level at which $W(x)=0$, results in most cases in a high transition temperature, but not necessarily the maximal possible for a given compound.

The conductivity due to the *degenerate* ξ carriers should be of a regular Fermi-liquid-type $\sigma_{xx}^\xi\propto\tau_\xi$. We note however that strongly underdoped systems undergo a metal-insulator transition (MIT). As the level of the chemical potential increases with a decreasing number of holes, it crosses the mobility threshold. To include this process in our model we take in Eq. (1) the transport relaxation rate of the ξ component to be a function of energy and temperature,[23] $\tau_\xi(T,\epsilon)=\tau_{\rm tr}(T)\theta(E_c-\epsilon)$, with $\tau_{\rm tr}(T)\sim\hbar/k_BT$, and $\theta(y)$ being the step function. E_c is the mobility threshold: only the holes with energy less than E_c contribute to transport. This crude approximation does not take into account hopping of localized carriers, but it is sufficient for our purposes here. Thus we obtain,

$$\sigma_{xx}^\xi=\frac{2e^2u^2(\mu)\nu_\xi\hbar}{k_B}\frac{1}{T}\frac{1}{e^{\beta(\mu-E_c)}+1}. \tag{7}$$

To arrive at Eq. (7), it was assumed that $u^2(\epsilon)\nu_\xi\equiv\Sigma_{\mathbf{k}}v_{x,\xi}^2(\mathbf{k})\delta(\epsilon-\epsilon_\xi(\mathbf{k}))$ is a slowly varying function of energy.

IV. DOPING AND TEMPERATURE DEPENDENCE OF IN-PLANE RESISTIVITY

To illustrate the details of temperature and doping variations of $\rho_{ab}(T,x)=(\sigma_{xx}^\xi+\sigma_{xx}^\eta)^{-1}$ given by Eqs. (4) and (7), we discuss below semiquantitatively the following cases:

(a)''optimally doped'' regime: the range of doping where $|W(x)|/T \sim 1$;
(b) Strongly ''underdoped'' regime: $W>0$; $W(x)/T>1$, and
(c) Strongly ''overdoped'' regime: $W<0$; $|W(x)|/T>1$.

A. Optimally doped regime

When the chemical potential is sufficiently below the mobility threshold $\exp\{\beta(\mu-E_c)\} \ll 1$, $\rho_{ab}(T)$ is given by

$$\rho_{ab} \approx \frac{AT}{\alpha+\Phi(W/T)}, \tag{8}$$

where $A=mk_B/(2e^2\hbar\nu_\eta\tilde{E})$, $\alpha=mu^2(\mu)\nu_\xi/(\tilde{E}\nu_\eta)$, and $\Phi(W/T)=\ln(1+Z)$, with Z given by Eq. (5). For $W=0$ the fugacity is T independent with the value $Z_0<1$ determined by the ratio of DOS λ in two subbands: $Z_0(1+Z_0)^\lambda=1$. Correspondingly, the chemical potential is positive (at all temperatures above the top of the lower band) and changes with temperature: $\mu=T\ln Z_0^{-1}$. Resistivity is linear in temperature with zero intercept. Both components of conductivity are of the same order of magnitude and have $1/T$ dependence. The smaller number of nondegenerate quasiparticles, Eq. (3), $n_\eta \propto T\ln(1+Z_0)$ is compensated by their higher mobility $\sim 1/T^2$.

Near threshold doping, $x \approx x_0$, so that $|W(x)| \ll T$, and

$$\rho_{ab} \approx A_1(T+T_0); \quad T_0=\gamma W(x), \tag{9}$$

where $A_1=A/[\alpha+\Phi(0)]$, and $\gamma=|\Phi'(0)|/[\alpha+\Phi(0)]$. In this limit ρ_{ab} is linear in T, with a small *positive* or *negative* intercept. The sign of the intercept of the linear extrapolation indicates whether the system is slightly underdoped or overdoped. As we will see below, at temperatures $T<|W|$ the resistivity deviates from Eq. (9). Positive intercept at $W>0$ is a precursor of the freezing out of the η component (opening of the pseudogap), while the negative intercept at $W<0$ is a precursor of the crossover from linear to quadratic T dependence at $T<|W|$. If the critical temperature is high enough, $T_c>|W|$, these crossovers are hidden by the onset of superconductivity and the normal-state resistivity is described by Eq. (9) at all temperatures above T_c.

Bilayer cuprates with maximal critical temperature typically have linear T dependence with zero or very small intercepts. For example, in $YBa_2Cu_3O_{7-\delta}$ crystals with zero-resistance temperature near 92 K, the resistivity is described by $\rho_{ab}=\alpha T+\beta$ (Ref. 24) with small *negative* intercepts β. The corresponding values of $|T_0| \sim 10-25$ K (see details in Ref. 25). It is important to point out that in our model spin susceptibility χ_s and the linear term in electronic entropy S/T are also functions of $W(x)/T$.[9] Thus, in the regime where the model gives linear resistivity, χ_s and S/T are temperature independent. These are the features of optimally doped (in conventional sense) cuprates with maximal or nearly maximal T_c. It may be noted that in this model, optimal doping corresponds to the situation when the chemical potential is very near the top the submerged band, so that the holes in this band remain nondegenerate at all temperatures down to T_c; Figs. 1(a) and 1(b).

B. Moderately and strongly underdoped regime

Reduction of the number of holes n_h by doping raises μ appreciably above the top of the lower subband. If $W(x)$ is such that at room temperature $W(x)/T \sim 1$, but T_c is low enough, so that $\exp\{-W(x)/T_c\} \ll 1$, freezing out of the η component of the charge carriers will have a notable effect on the T dependence of resistivity in the temperature range $T_c<T \lesssim 300$ K. This corresponds to the underdoped regime in which $\rho_{ab}(T)$ exhibits a *crossover* between two temperature ranges. For $T \gg W$, $\rho_{ab}(T)$ is still approximately linear ($\rho_{ab}=A_1T+B$) with a large positive *apparent* intercept $B=A_1T_0 \propto W$, Eq. (9). At lower temperatures ($T \ll W$) $\Phi(W/T) \approx \exp(-W/T)$ and the nondegenerate component freezes out. Thus, the T dependence of ρ_{ab} can be approximately expressed as

$$\rho_{ab} \approx \begin{cases} A_1(T+T_0); & T>T^* \\ A_2T; & T<T^* \end{cases} \tag{10}$$

with $A_2=A/\alpha>A_1$ and T_0 the same as in Eq. (9). Note that below T^*, ρ_{ab} is still linear in T, but with a *greater* slope than at higher temperature and *zero intercept*. The curve $\rho_{ab}(T)$ acquires a characteristic downward curvature and the change of slope $d\rho_{ab}/dT$ occurs around a $T^*(x) \propto W(x)/|\ln(\alpha)|$. Since the change of slope results from freezing out of one of the components of charge carriers, it correlates with the decrease in $\chi_s(T)$ and entropy.[9]

As the number of holes decreases, the chemical potential monotonically rises above the top of the submerged subband and the change of slope of $\rho_{ab}(T)$ takes place at progressively higher temperatures. When μ goes above the mobility threshold E_c, the in-plane resistivity also shows a minimum and an upturn at sufficiently low temperatures $T<\mu-E_c$:[26]

$$\rho_{ab} \approx \begin{cases} A_1(T+T_0); & T>T^* \\ A_2T(e^{\beta(\mu-E_c)}+1); & T<T^*. \end{cases} \tag{11}$$

C. Overdoped regime

The overdoped regime in our model corresponds to the situation when the total number of holes increases above the level at which resistivity is linear with zero intercept, Eq. (9), and therefore the chemical potential goes below the top of the lower band, Figs. 1(a) and 1(b). This corresponds to $x<x_0$ and $W(x)<0$. At sufficiently low temperatures $T \lesssim |W(x)|/(1+\lambda)$ the η component also becomes degenerate. For $x<x_0$ and $|W(x)| \gg T$ the fugacity $Z \gg 1$; Eq. (5) yields $\mu \approx W/(\lambda+1)$, and $\Phi(W/T) \approx |\mu|/T$. Thus $\rho_{ab}(T)$ acquires the characteristic *upward* curvature:

$$\rho_{ab} \approx \frac{AT^2}{\alpha T+|\mu|}. \tag{12}$$

Notice that a characteristic energy $|\mu|$, which determines the curvature of $\rho_{ab}(T)$ reappears in the overdoped regime and increases with overdoping. The manifestation of this new energy scale in the overdoped crystals and its physical meaning are clearly different from those in the underdoped systems. If we define $T^* \approx |\mu|/\alpha=|W(x)|/\alpha(\lambda+1)$, the new crossover temperature corresponds to transition from approximately linear with *negative* intercept T dependence at

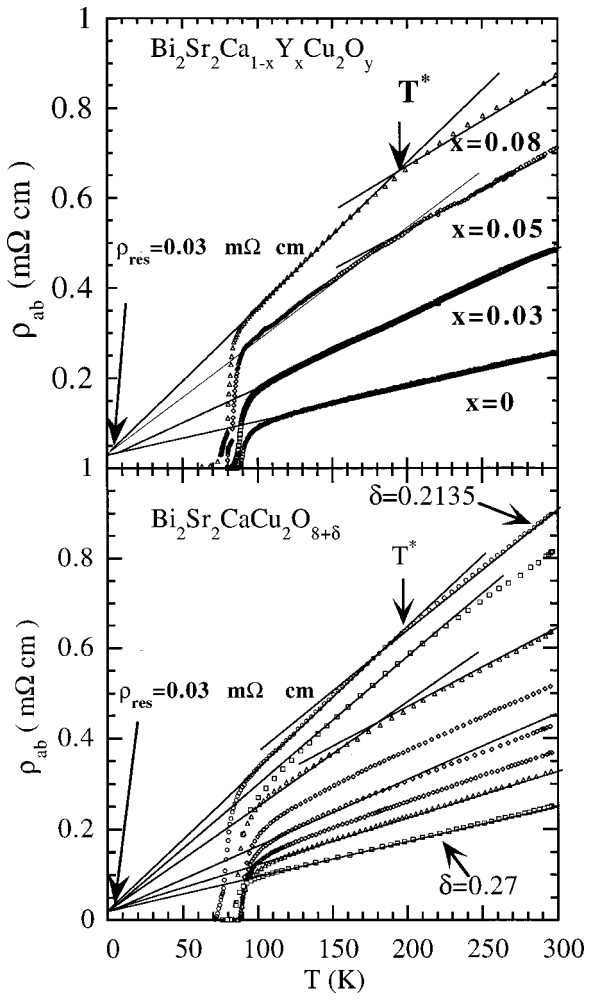

FIG. 2. Resistivity of $Bi_2Sr_2Ca_{1-x}Y_xCu_2O_2$ (upper panel) and $Bi_2Sr_2CaCu_2O_{8+\delta}$ (lower panel) crystals. The temperature T^* is indicated by the change of slope of the linear asymptotes. Note that the lower temperature asymptotes converge at the small residual resistivity $\rho_{res} \approx 0.03\,\mathrm{m}\Omega$ cm. This is characteristic of only these crystals. Otherwise, the data in Fig. 1(c) and Figs. 2 are very similar in T dependence and the values of the resistivity.

$T > T^*$ to quadratic at $T < T^*$. This characteristic temperature increases with overdoping.

V. COMPARISON TO DATA

A. Under and optimally doped cuprates

The in-plane resistivity for Pr-doped single crystals of $Y_{1-x}Pr_xBa_2Cu_3O_{7-\delta}$ (Ref. 3) is shown in Fig. 1 (main panel). In Fig. 2 we show the same for single crystals of $Bi_2Sr_2Ca_{1-x}Y_xCu_2O_y$ (Ref. 2) (upper panel), and $Bi_2Sr_2CaCu_2O_{y+\delta}$ (Ref. 1) (lower panel). These are bilayer crystals exhibiting evolution with doping from the optimally doped (in terms of critical temperature) to the underdoped regime. The overall T dependence of all of these systems and their evolution with doping are similar. Samples with maximal T_c show linear $\rho_{ab}(T)$ with zero or very small positive or *negative* intercepts (see also Ref. 24). The characteristic change of slope at T^* is obvious in strongly underdoped samples with the T dependence in accordance with Eq. (10), shown by the straight lines. Note that $Bi_2Sr_2Ca_{1-x}Y_xCu_2O_y$ and $Bi_2Sr_2CaCu_2O_{y+\delta}$ crystals exhibit small *genuine* residual resistivity $\rho_{res} \approx 0.03\,\mathrm{m}\Omega$ cm in contrast with *apparent* intercepts of the high-temperature (above T^*) asymptotes, which are much greater and increase with underdoping. The real residual resistivity such as that in Fig. 2 can be incorporated into our model by taking the relaxation rate τ_ξ^{-1}, which determines the resistivity below T^* in the form $\hbar\tau_\xi^{-1} \sim k_B T + \hbar\tau_0^{-1}$, instead of Eq. (1) ($\tau_0^{-1} = \text{const}$ and reflects the scattering rate from defects or impurities). In $Y_{1-x}Pr_xBa_2Cu_3O_{7-\delta}$ samples there is no indication of the true residual resistivity and the underdoped sample such as $x = 0.29$ has linear T dependence below T^* in accordance with Eq. (10).

In $Bi_2Sr_2Ca_{1-x}Y_xCu_2O_y$ the transformation from optimally doped to underdoped regime is the result of hole filling due to Y^{3+} substitution for Ca^{2+}. The Ca-Y atoms are sandwiched inside the bilayer between the two CuO_2 sheets. In $Bi_2Sr_2CaCu_2O_{y+\delta}$ the effect of changing oxygen content is similar to that in $YBa_2Cu_3O_{7-\delta}$, namely the decreasing concentration of oxygen in the blocking layers located outside of the bilayers also reduces the number of holes on the bilayers.

The mechanism by which Pr substitution drives $Y_{1-x}Pr_xBa_2Cu_3O_{7-\delta}$ into the underdoped regime has been a subject of intensive debate, which is not yet resolved (see Ref. 27 and references therein). While high-energy spectroscopy and some band-structure calculations indicate a Pr^{3+} state, transport, neutron diffraction, optical, and Mossbauer spectroscopies indicate a Pr valence greater than 3^+.[28] But when we compare the resistivities in Fig. 2 with those in Fig. 1, we see that the temperature dependence and even the values of the resistivities in these crystals are very similar. Since the evolution of resistivity of $Y_{1-x}Pr_xBa_2Cu_3O_{7-\delta}$ is very similar to that of $Bi_2Sr_2Ca_{1-x}Y_xCu_2O_y$ and $Bi_2Sr_2CaCu_2O_{y+\delta}$ (in which the hole filling mechanism is not in doubt), we have chosen to use the data in Fig. 1 to compare with our model results.

Figure 1(c) shows the data[3] along with theoretical curves for $\rho_{ab} = \sigma_{ab}^{-1}$, where σ_{ab} is given by Eqs. (4), (5), and (7):

$$\sigma_{ab} = \frac{a(x)}{T}\,\frac{1}{e^{\beta(\mu - E_c)} + 1} + \frac{b(x)}{T}\,\Phi\left(\frac{W}{T}\right). \qquad (13)$$

The fitting shows that the parameter $a(x) = \alpha/A$ [see Eq. (8) for definition] decreases with increasing Pr concentration indicating that the average velocity $u^2(\mu)$ on the Fermi surface decreases monotonically. On the contrary, $b(x) = 1/A$ increases with x.[29] For all doping levels, the ratio of DOS in two subbands λ is taken equal to 2.3, the same value that was found from fitting the susceptibility in a bilayer cuprate $TlSr_2Lu_{1-x}Ca_xCu_2O_x$.[9] The fitting also determines the mobility threshold $E_c \approx 744$ K, so that the sample with $x = 0.42$ ($\mu \approx W = 800$ K) is on the insulating side very near the metal-insulator transition. The sample with $x = 0.51$ is well into the insulating regime. We have not taken variable range hopping into account, which is why the resistivity given by Eq. (13) diverges more strongly at low temperature than the data for $x = 0.51$.

The parameter $W(x)$ which determines the fugacity [Eq. (5)] is shown in Fig. 3(a) along with the empirical crossover temperature T^* determined by the change of slope of the resistivity. The doping dependence of $W(x)$ is indeed linear,

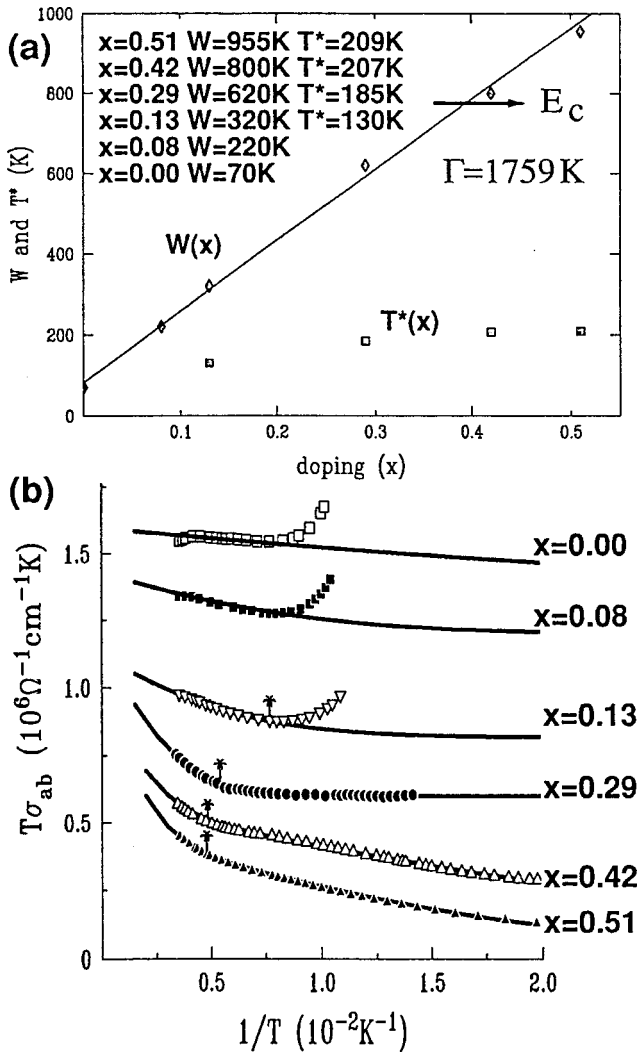

FIG. 3. (a) Doping dependence of $W(x)$ (diamonds). The solid line is a linear fit $W(x)=\Gamma(x-x_0)$. The value of the threshold doping $x_0\approx-0.05$. The arrow indicates the mobility threshold $E_c \approx 744$ K. Also shown are the empirical crossover temperatures $T^*(x)$ (squares), indicated in Fig. 1(c). (b) The data of Fig. 1(c) plotted as $T\sigma_{ab}$ vs $1/T$. The palm signs correspond to the same temperature T^* as in Fig. 1(c). The solid lines represent the same theory as in Fig. 1(c), Eq. (13).

in accordance with Eq. (6). The same linear dependence of $W(x)$ was found in a different bilayer cuprate from the analysis of the spin susceptibility.[9]

It should be noted that in the *strongly underdoped* regime [$Z\ll 1$, Eq. (5)] the gap in the spectrum of the η excitations is given by $W(x)$, since $Z=\exp\{-\mu/k_BT\}\approx\exp\{-W/k_BT\}$. This gap manifests itself in the T dependence of the resistivity as the change of slope resulted from the freezing out of the η component. The crossover temperature is determined approximately by the condition following from Eq. (8):

$$\alpha\approx\exp\{-W/T^*\}. \tag{14}$$

If $\alpha=a(x)/b(x)$ was constant, the crossover temperature would scale proportionately to the gap. However, as discussed above, $a(x)$ decreases and $b(x)$ increases with x, so that

$$\alpha=\frac{mu^2(\mu)\nu_\xi}{\tilde{E}\nu_\eta} \tag{15}$$

strongly decreases with underdoping due to decreasing Fermi energy (mu^2) in the degenerate band and the increasing lifetime of the η particles manifested in increasing $\tilde{E}$,[29] Eq. (1). The fitting shows that the value of α decreases from 2.2 at $x=0$ to 0.4 for $x=0.29$. Therefore, $T^*(x)\approx W(x)/|\ln\alpha(x)|$ is appreciably smaller than W, increases with x not at the same rate and, as Fig. 3(a) demonstrates, does not have the linear dependence. Moreover, since T^* is defined as a temperature at which the slope of $\rho_{ab}(T)$ changes, it cannot be identified in the samples close to optimal doping. In these samples the existence of the small energy scale manifests itself through the intercept of the linear dependence [positive or negative dependening on the sign of $W(x)$]. Below, in Sec. VI we discuss a different way to determine empirically the underlying energy scale from experimental data.

The idea that the change of slope $d\rho_{ab}/dT$ at T^*, as indicated in Figs. 1 and 2, results from the freezing out of one component of charge carriers can be illustrated even more convincingly by plotting $T\sigma_{ab}$ versus $1/T$; see Eq. (13). With the overall $1/T$ dependence of $\sigma_{ab}(T)$ removed, the data in Fig. 3(b) for samples with $x=0-0.29$ clearly demonstrate the Arrhenius-type dependence $T\sigma_{ab}\approx a+b\Phi(W/T)$ with $\Phi(W/T)\approx\exp(-W/T)$. The empirical crossover temperature T^* is the same as in Fig. 1(c), and it roughly corresponds to the transition from the two carrier regime (ξ and η) at higher temperatures to a single carrier regime (ξ) at $T<T^*$. The upturns at low temperatures are the result of the onset of superconductivity. In the samples with $x=0.42$ and 0.51, which are on the insulating side of MIT, $T\sigma_{ab}(T)$ does not saturate at low temperatures. Here too, T^* is the same temperature as in Fig. 1(c). The solid curves are calculated using Eq. (13) with the same parameters, $a(x)$, $b(x)$, and $W(x)$, as in Figs. 1(c) and 3(a).

B. Overdoped cuprates

We present in Figs. 4 the calculated resistivity in overdoped regime. In our model, the overdoped regime corresponds to the chemical potential going below the top of the lower band, Figs. 1(a) and 1(b). This corresponds to negative values of $W(x)$ and of the chemical potential μ, which is measured with respect to the top of the lower subband. The excitations in the lower band are no longer gapped and a second Fermi surface would form at temperatures $T\ll|\mu|=|W|/(\lambda+1)$, see Eq. (5). However, if $|\mu|$ is small enough (the crystal is not too overdoped), the η excitations will remain nondegenerate in the normal state (above T_c). Therefore, the small energy parameter $W(x)<0$, which determines the temperature dependence of resistivity and susceptibility in the overdoped regime has different meaning and different manifestations compared to that in the underdoped regime.

Figure 4 (upper panel) shows the calculated [using Eq. (13)] resistivity for three values of $W=-220$, -320, and -800 K that correspond to progressively greater overdoping. For comparison, the data from Fig. 1 are also included (optimally doped and slightly underdoped samples with $x=0$ and 0.08). For calculations of the overdoped resistivities the

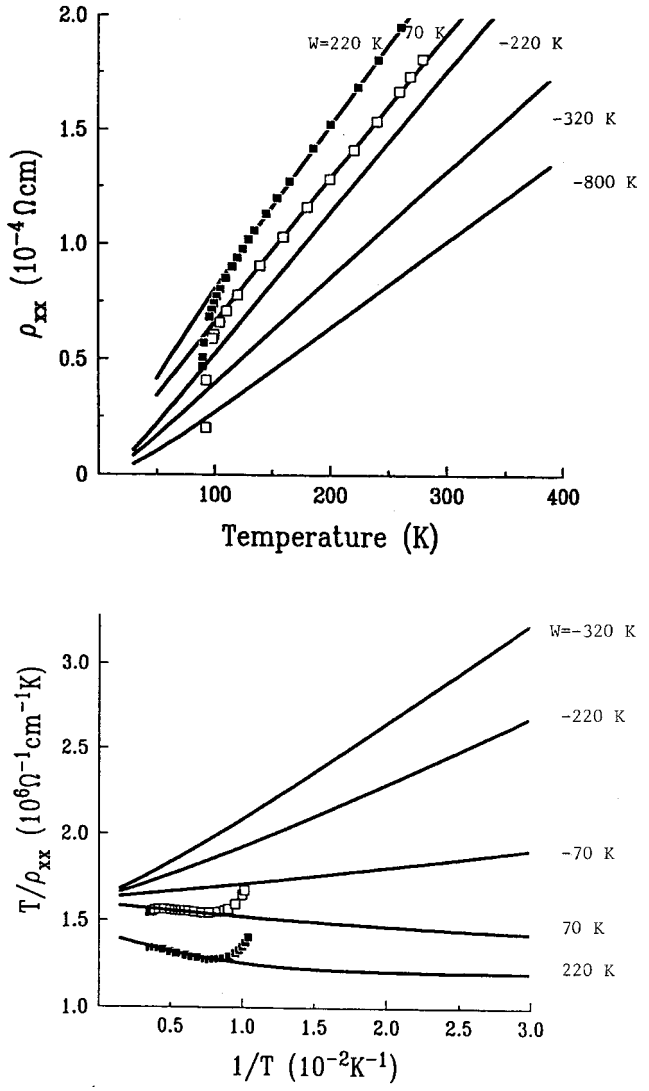

FIG. 4. Upper panel: Resistivity in the overdoped regime calculated using Eq. (13) ($W=-220$, -320, and -800 K). For comparison, the data for optimally and slightly under-doped samples ($x=0$ and 0.08) from Fig. 1(c) are also shown ($W=70$ and 220 K, respectively). Lower panel: Same data and calculations presented as $T\sigma_{ab}$ vs $1/T$. The low-temperature asymptotes are described as $T\sigma_{ab}\approx a+b|\mu|/T$ in agreement with Eq. (12). High-temperature slopes $\partial \ln(T\sigma_{ab})/\partial(1/T)$ correlate in sign and value with $-W(x)$.

values of parameters a and b in Eq. (13) were taken the same as for the sample $x=0$. Note that the energy scale, which governs the deviation of resistivity from linear T dependence in the overdoped regime, is $|\mu|=|W|/(\lambda+1)$, so that for $\lambda=2.3$ even $W=-800$ K still corresponds to relatively small $|\mu|\approx 242$ K. We see that the high-temperature dependence of ρ_{ab} is approximately linear, with an apparent negative intercept. As discussed in Sec. IV C, this negative intercept is a precursor to the crossover to superlinear (quadratic) T dependence at temperatures $T\ll|\mu|$. The small negative intercepts characterize the T dependence of the optimally doped clean crystals of $YBa_2Cu_3O_{7-\delta}$.[24,25] When $T_c\sim|\mu|$, the crossover to quadratic T dependence of resistivity at low temperatures is obscured by the onset of superconductivity. Overall, the T dependence of resistivity shown in Fig. 4 is similar to that of strongly overdoped crystals of $Tl_2Ba_2CuO_{6+\delta}$.[4,6]

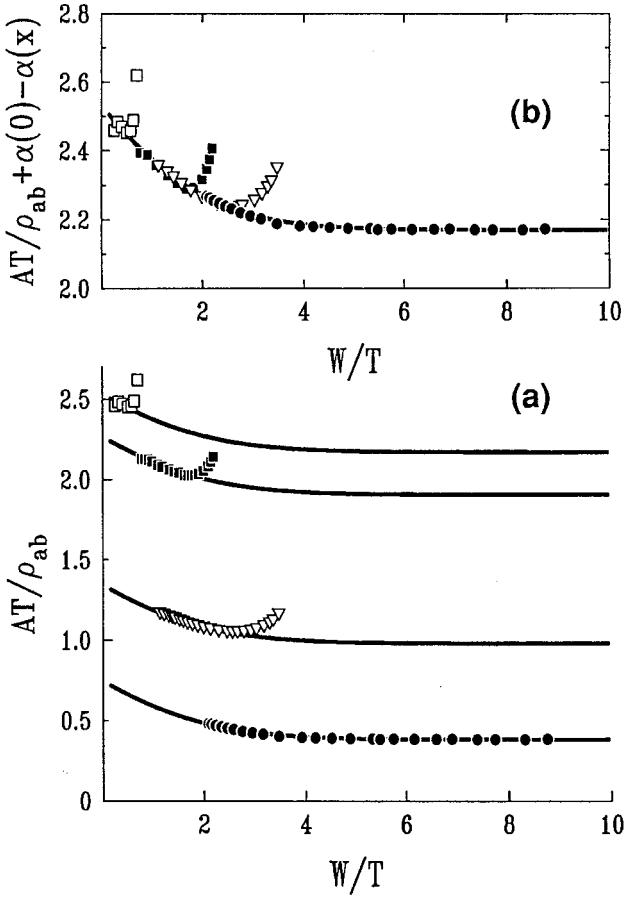

FIG. 5. (a) To demonstrate scaling, $A(x)T\sigma_{ab}$ is plotted vs W/T. The solid lines are identical curves $\alpha(x)+\Phi(y)$ shifted with respect to each other due to different $\alpha(x)$; the symbols are the same as in Fig. 1(c). (b) When the points are shifted upward by $\alpha(0)-\alpha(x)$ they form a single continuous curve.

On the lower panel of Fig. 4 the same calculations and data are presented as T/ρ_{ab}, similar to Fig. 3(b). This shows the correlation in sign between the slope $\partial(T\sigma)/\partial(1/T)$ and the sign of W. The low-temperature behavior of overdoped $T\sigma_{ab}$ can be roughly approximated as $a+b'/T$ with increasing with overdoping coefficient $b'\approx b|\mu|$, see Eqs. (13) and (5).

C. Scaling

Sufficiently far from the mobility threshold E_c (on the metallic side of MIT), $W(x)$ is the sole parameter governing the temperature dependence of σ_{ab}, Eq. (8). In this regime the model predicts a three-parameter scaling of the form

$$A(x)T\sigma_{ab}=\alpha(x)+\Phi(W(x)/T). \tag{16}$$

This approximate scaling is illustrated in Fig. 5. The lower panel shows the same data as in Fig. 3(b), only multiplied by parameter $A(x)=b^{-1}$, determined by fitting the data with Eq. (13), and plotted vs $W(x)/T$. The solid curves are the right-hand sides of Eq. (16): $\alpha+\Phi(y)$, where $\Phi(y)=\ln(1+Z)$ with $Z(1+Z)^{\lambda}=e^{-y}$. These curves are defined for positive (underdoped) and negative (overdoped) values of $y=W/T$. In Fig. 5 only the positive branch is shown. These identical curves are shifted due to the different values of α,

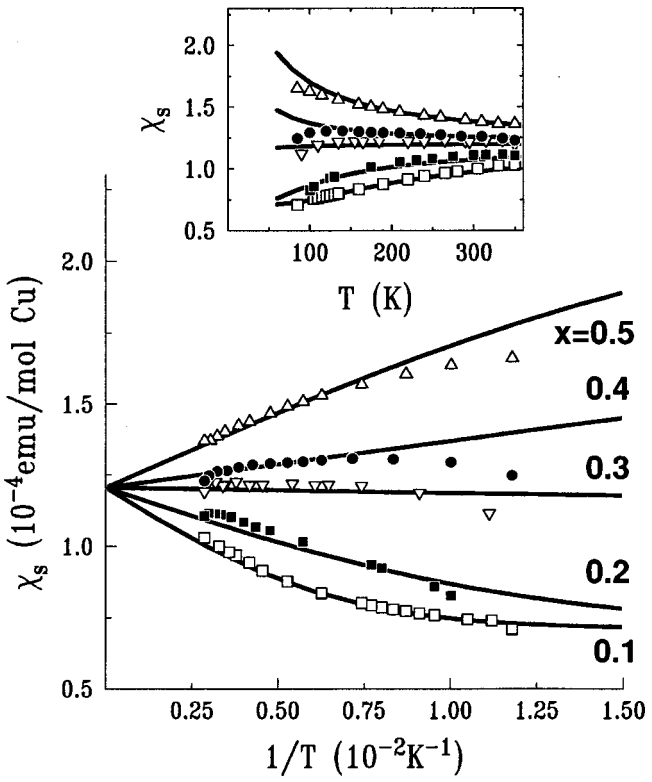

FIG. 6. Susceptibility of $TlSr_2Lu_{1-x}Ca_xCu_2O_y$ ($x=0.1$ is strongly underdoped and $x=0.5$ strongly overdoped crystals). The solid curves are calculated within our model. High-temperature slopes, Eq. (17) correlate with the values of $-W(x)$. The inset shows the same data and theory plotted vs temperature.

and in the upper panel they are collapsed on one curve by the upward shift by $\alpha(0)-\alpha(x)$. A similar scaling, which includes the data for underdoped and overdoped crystals was found for the spin susceptibility in another bilayer cuprate.[9]

VI. CONCLUDING REMARKS

We have presented what we believe to be a plausible explanation for the observed characteristic crossover temperature T^* in in-plane resistivity in biplanar high-T_c cuprates. We have also shown that the same framework can, in a natural fashion, account for the Fermi-liquid-like behavior in the overdoped regime as well. One of the key points of this paper is to show that these features in the under, optimal, and overdoped bilayer cuprates are governed by an underlying relatively small energy scale. In the underdoped regime, we believe this energy scale to be related to what is referred to as the ''pseudogap'' in literature. This can be large in the strongly underdoped crystals and vanish at optimal doping. In the overdoped regime the characteristic energy scale appears in the form of a Fermi energy of the second emerging Fermi surface that increases with overdoping. In addition to in-plane resistivity, this type of evolution is also evident in the data on the spin susceptibility χ_s (Refs. 7,9) and electronic entropy. To demonstrate this explicitly, and for the sake of completeness, we reproduce in Fig. 6 the electronic susceptibility data,[7] that were analyzed in Ref. 9. The susceptibility of the $TlSr_2Lu_{1-x}Ca_xCu_2O_y$ crystals that evolve from underdoped ($x=0.1$) to overdoped ($x=0.5$) regime changes in a predictable manner consistent with the behavior of the susceptibility in other cuprates, such as $La_{2-x}Sr_xCuO_4$.[5,30] The optimal doping corresponds to a practically T independent χ_s. Outside of optimal doping the susceptibility becomes noticeably T dependent within the range of temperature $T_c<T\leqslant 300$ K. This requires a certain energy parameter to be present to scale the temperature: $\chi_s=\chi_s(T/E^*)$, with the absolute values of E^* roughly within the same interval as the temperature. An empirical characterization of the doping-dependent energy scale E^* is the high-temperature slope of χ_s as seen in Fig. 6:

$$E^*_\chi(x)=\left.\frac{\partial \ln \chi_s}{\partial(1/T)}\right|_{T=300\ \mathrm{K}}. \tag{17}$$

The subscript E^*_χ indicates E^* obtained from the susceptibility data. The overdoped and underdoped regimes are characterized by the opposite sign of E^*, which reflects the opposite curvatures of $\chi_s(T/E^*)$.

The resistivity data presented in Figs. 1(c), 2, and 4 (upper panel) demonstrate the same phenomenon as in Fig. 6. The optimal doping is characterized by a zero energy parameter and a strictly linear resistivity with zero intercepts. The small apparent intercepts (positive or negative), which appear in the extrapolations of the high-temperature T dependence of ρ_{ab} in underdoped and overdoped samples, respectively, increase in absolute values, and at greater under-or overdoping evolve into a noticeable curvature of resistivity. Since the strictly linear dependence of ρ_{ab} corresponds to zero pseudogap, these intercepts and curvatures require an underlying energy scale, which increases on both sides of optimal doping. This becomes especially obvious when we remove the overall $1/T$ dependence of conductivity as shown in Figs. 3(b) and 4 (lower panel). We can also define the characteristic energy from the resistivity data as the high-temperature slope of $T\sigma_{ab}$:

$$E^*_\rho(x)=\left.\frac{\partial \ln(T\sigma_{ab})}{\partial(1/T)}\right|_{T=300\ \mathrm{K}}. \tag{18}$$

Comparing our results for spin susceptibility,[9] (Fig. 6) with Figs. 3(b) and 4 (lower panel) we find that the empirical energy scales from susceptibility and resistivity correlate with each other at all doping levels.

In our model, the underlying energy scale, related to the crossover temperature T^*, is the energy difference between the top of the lower band and the level of the chemical potential, which changes with doping, Figs. 1(a) and 1(b). In the underdoped regime the chemical potential is above the top of the submerged subband and the excitations in this band are gapped. The activation energy $\mu\approx W(x)$ determines the temperature at which one component of the charge carriers freezes out. This leads to the decrease at low temperature of the spin susceptibility,[5,9] the linear term in electronic entropy,[9] and $T\sigma_{ab}$, Fig. 3(b).

The overdoped regime corresponds to the chemical potential going below the top of the submerged subband [$\mu\approx W/(\lambda+1)<0$], so that η excitations are no longer gapped. Instead, the energy scale here, $|\mu|$, is the small Fermi energy of the emerging second Fermi surface. Correspondingly, the manifestations of this emerging second Fermi sur-

face are very different from those of the gap in the underdoped phase. As temperature decreases well below $|\mu|$ the carriers in the second subband go from being nondegenerate to degenerate. As a result, the susceptibility,[5,9] the linear term in electronic entropy,[9] and $T\sigma_{ab}$, Fig. 4 increase with decreasing temperature. A consequence of this model is that the maximal critical temperature is reached in the crystals in which the chemical potential is very close to the top of the lower band. Therefore, one component of charge carriers undergoes pairing while remaining *nondegenerate* at T_c.

Finally, while we do not yet have a good microscopic calculation that explicitly gives rise to the degenerate and nondegenerate carriers, we speculate on a possible origin for the two 2D subbands. This may result from the coupling between two CuO_2 layers within a bilayer.[9,20] The quasiparticles in the lower subband are even combinations of the atomic orbitals, $|\eta\rangle \propto |1\rangle + |2\rangle$, while the upper, degenerate, band is comprised of odd combinations, $|\xi\rangle \propto |1\rangle - |2\rangle$. Eigenstates $|1\rangle$ and $|2\rangle$ are centered on the respective layers. Recently, it has become possible to separate the effects of even and odd excitations on the spin susceptibility in underdoped $YBa_2Cu_3O_{7-\delta}$.[31] A brief summary of these results is that in the *normal state* of the underdoped system the ''even'' spectrum is truly gapped, while the ''odd'' spectrum is not. This is expected from our scenario depicted in Fig. 1(b). Experiments such as Ref. 31 merit separate analysis, and we only point out here that the different behavior of the even and odd contributions to susceptibility give additional support to our model and are consistent with the previous results for susceptibility.[9]

ACKNOWLEDGMENTS

We thank C. C. Almasan, T. Watanabe, K. Q. Ruan, and their colleagues (Refs. 1–3) for making available to us the resistivity data. The work has been partially supported by a grant from the Ohio Research Challenge.

[1] T. Watanabe, T. Fujii, and A. Matsuda, Phys. Rev. Lett. **79**, 2113 (1997).
[2] K. Q. Ruan, Y. Feng, C. Y. Wang, X. H. Chen, and L. Z. Cao, Physica C **282-287**, 1165 (1997).
[3] M. B. Maple, C. Almasan, C. Seaman, S. H. Han, K. Yoshiara, M. Buchgeister, L. M. Paulius, B. W. Lee, D. A. Gajewski, R. F. Jarnim, C. R. Fincher, Jr., G. Blanchet, and R. Guertin, J. Supercond. **7**, 97 (1994).
[4] A. P. Mackenzie, S. R. Julian, D. C. Sinclair, and C. T. Lin, Phys. Rev. B **53**, 5848 (1996).
[5] B. Batlogg *et al.*, Physica C **235-240**, 130 (1994), and references therein.
[6] T. Manako, Y. Kubo, and Y. Shimakawa, Phys. Rev. B **46**, 11 019 (1992).
[7] T. Kondo, Y. Kubo, Y. Shimakawa, and T. Manako, Phys. Rev. B **50**, 1244 (1994).
[8] J. W. Loram *et al.*, Phys. Rev. Lett. **71**, 1740 (1993).
[9] G. A. Levin and K. F. Quader, Physica C **258**, 261 (1996); Phys. Rev. B **53**, R530 (1996).
[10] C. M. Varma *et al.*, Phys. Rev. Lett. **63**, 1996 (1989); D. Newns *et al.*, *ibid.* **73**, 1695 (1994).
[11] B. Stojkovic and D. Pines, Phys. Rev. Lett. **76**, 811 (1996), and references therein.
[12] G. Baskaran, Z. Zou, and P. W. Anderson, Solid State Commun. **63**, 973 (1987); S. Doniach and M. Inui, Phys. Rev. B **41**, 6688 (1990); V. Emery and S. Kivelson, Nature (London) **374**, 434 (1995); P. Coleman, A. J. Schofield, and A. M. Tsvelik, Phys. Rev. Lett. **76**, 1324 (1996).
[13] H. Alloul, T. Ohno, and P. Mendels, Phys. Rev. Lett. **63**, 1700 (1989); J. Rossat-Mignod *et al.*, Physica B **169**, 58 (1991).
[14] L. D. Rotter *et al.*, Phys. Rev. Lett. **67**, 2741 (1991).
[15] A. Carrington, A. P. Mackenzie, C. T. Lin, and J. R. Cooper, Phys. Rev. Lett. **69**, 2855 (1992); R. Hlubina and T. M. Rice, Phys. Rev. B **51**, 9253 (1995).
[16] L. B. Ioffe and A. J. Millis, Phys. Rev. B **58**, 11 631 (1998).
[17] G. A. Levin and K. F. Quader, Phys. Rev. B **46**, 5872 (1992).
[18] N. P. Ong, in *Physical Properties of High Temperature Superconductors II*, edited by D. M. Ginsberg (World Scientific, Singapore, 1990), and references therein; V. Z. Kresin and S. A. Wolf, Solid State Commun. **63**, 1147 (1987).
[19] P. W. Anderson, Phys. Rev. Lett. **67**, 2092 (1991).
[20] K. F. Quader and G. A. Levin, Philos. Mag. B **74**, 611 (1996).
[21] J. P. Rice, J. Giapintzakis, D. M. Ginsberg, and J. M. Mochel, Phys. Rev. B **44**, 10 158 (1991).
[22] M. Sasaki, G. X. Tai, S. Tamura, and M. Inoue, Phys. Rev. B **46**, 1138 (1992).
[23] P. W. Anderson, Phys. Rev. **109**, 1492 (1958); **109**, 1972 (1958); Proc. Natl. Acad. Sci. U.S.A. **69**, 1097 (1985).
[24] T. A. Friedmann *et al.*, Phys. Rev. B **42**, 6217 (1990).
[25] G. A. Levin and K. F. Quader, J. Low Temp. Phys. **89**, 551 (1992).
[26] Equation (11) overestimates the resistivity at low temperatures ($T \ll \mu - E_c$), where the conductivity due to activated holes will be negligible, and hopping (as well as variable range hopping) $\sigma_h \approx \sigma_0 \exp[-(T_0/T)^\nu]$ ($\nu \leqslant 1$) will dominate conductivity.
[27] M. Merz *et al.*, Phys. Rev. B **55**, 9160 (1997).
[28] A. A. Moolenaar *et al.*, Physica C **267**, 279 (1996), and references therein.
[29] The increase in $b(x)$ stems from that of $\tilde{E}(x)$ in the lifetime $\tau_\eta = \hbar\tilde{E}/(k_B T)^2$. The increase in the lifetime of the carriers in the lower subband is consistent with τ_η being determined by inelastic scattering $\eta\xi \rightarrow \eta\xi$ and $\eta\eta \rightarrow \eta\eta$ since the number of *mobile* holes in both bands apparently decreases with increasing Pr concentration.
[30] T. Nakano *et al.*, Phys. Rev. B **49**, 16 000 (1994).
[31] H. F. Fong *et al.*, Phys. Rev. B **61**, 14 773 (2000), and references therein.